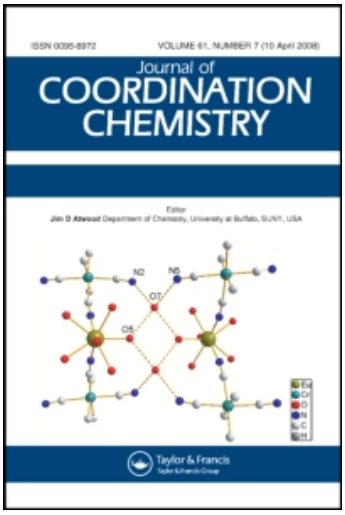

Journal of Coordination Chemistry
Publication details, including instructions for authors and subscription information:
http://www.informaworld.com/smpp/title~content=t713455674

Synthesis, structure, and magnetic properties of bis(3-amino-2-chloropyridinium)tetrahalocuprate(II) [halide = Cl or Br]

Susan N. Herringer[a]; Mark M. Turnbull[a]; Christopher P. Landee[a]; Jan L. Wikaira[b]
[a] Carlson School of Chemistry and Biochemistry and the Department of Physics, Clark University, Worcester, MA 01610, USA [b] Department of Chemistry, University of Canterbury, Christchurch, New Zealand

To cite this Article Herringer, Susan N. , Turnbull, Mark M. , Landee, Christopher P. and Wikaira, Jan L.(2009) 'Synthesis, structure, and magnetic properties of **bis**(3-amino-2-chloropyridinium)tetrahalocuprate(II) [halide = Cl or Br]', Journal of Coordination Chemistry, 62: 6, 863 — 875
To link to this Article: DOI: 10.1080/00958970802395604
URL: http://dx.doi.org/10.1080/00958970802395604

Journal of Coordination Chemistry
Vol. 62, No. 6, 20 March 2009, 863–875

Taylor & Francis
Taylor & Francis Group

Synthesis, structure, and magnetic properties of *bis*(3-amino-2-chloropyridinium)tetrahalocuprate(II) [halide = Cl or Br]

SUSAN N. HERRINGER†, MARK M. TURNBULL*†, CHRISTOPHER P. LANDEE† and JAN L. WIKAIRA‡

†Carlson School of Chemistry and Biochemistry and the Department of Physics, Clark University, 950 Main Street, Worcester, MA 01610, USA
‡Department of Chemistry, University of Canterbury, Christchurch, New Zealand

(*Received 26 June 2008; in final form 1 August 2008*)

The reaction of CuX_2 (X = Cl or Br) with 3-amino-2-chloropyridine in aqueous acids (HX; X = Cl or Br) yields *bis*(3-amino-2-chloropyridinium)tetrachlorocuprate(II) and *bis*(3-amino-2-chloropyridinium)tetrabromocuprate(II). Both compounds have been characterized by IR, powder X-ray diffraction, single-crystal X-ray diffraction and temperature dependent magnetic susceptibility. The compounds are isomorphous and exhibit weak antiferromagnetic interactions.

Keywords: X-ray structure; Copper complexes; Magnetic properties; Tetrahalocuprates

1. Introduction

Continued interest in low-dimensional magnetic lattices has led to the study of compounds with the general formula $A_2[MX_4]$, where A is an organic cation, M is a 2+ transition metal ion and X is a halide (Cl or Br). The organic cation is usually a protonated base; known compounds have contained bases such as alkyl amines [1], substituted pyridines [2], or 2-aminopyrimidine [3]. The Cu(II) ion is an attractive source for the transition metal, M, because of its d^9 configuration and single unpaired electron, making it an S = ½ ion. The absence of a large internal magnetic field, indicated by a g-factor close to 2, allows the Cu(II) ion to follow an external magnetic field [4]. A number of complexes containing the tetrahalocuprate(II) have been reported in the literature where the halide is either chloride or bromide [5–7]. The crystal packing, and hence the distance of the Cu–X···X–Cu non-bonding contacts, is known to affect the magnetic susceptibility of such complexes [8].

Previously studied is a family of compounds, (2-amino-5-S-pyridinium)$_2$CuBr$_4$, where S = methyl, Cl, or Br [5-SAP] whose members are isostructural and exhibit antiferromagnetic interactions [9, 10]. The bulk and the length of the 5-substituent affect the

*Corresponding author. Email: Mturnbull@clarku.edu

ISSN 0095-8972 print/ISSN 1029-0389 online © 2009 Taylor & Francis
DOI: 10.1080/00958970802395604

packing motif of the compounds, and as a result have a significant effect on the exchange interactions within and between the layers [9]. The copper bromide tetrahedra are arranged in square lattices with the organic cations separating them. The 5-substituent on the pyridine ring is positioned within the CuX_4^{2-} containing layer, thereby separating the copper halide ions. Within the 5SAP family the order of decreasing magnetic interactions is shown by an increase in the size of the 5-substituent because the magnetic interactions occur through halide $\cdots$ halide contacts [9]. As the size of the substituent decreases, the copper bromide tetrahedra pack more tightly, giving a greater halide $\cdots$ halide overlap and therefore stronger magnetic exchange. The amine group, along with the pyridinium hydrogen, dictate this packing motif by hydrogen bonding to neighboring bromides [9]. As stated above, such changes in crystal packing affect the non-bonding halide-halide contacts and therefore the sign and magnitude of exchange interactions.

Related compounds include (2-amino-3-methylpyridinium)$_2CuX_4$ [X = Cl, Br] [11], (3-ammoniumpyridinium)CuX_4 [X = Cl, Br] [12], and (2,3-dimethylpyridinium)$_2CuBr_4$ which is known to be an antiferromagnetic ladder [13]. The 2-amino-3-methylpyridinium complex, being a 2-aminopyridinium compound, displays typical hydrogen bonding to the CuX_4 ions contributing to its tightly packed crystal lattice. (3-Ammoniumpyridinium)CuX_4 consists of layers of nearly square planar copper halide ions which are connected to the cations through N–H $\cdots$ X hydrogen bonds. The ammonium group forms three hydrogen bonds, one to a bridging halide and two to non-bridging halides, while the pyridinium–hydrogen forms bifurcated hydrogen bonds to two halides, one bridging and one non-bridging. These hydrogen bonding patterns cause the halide ions in adjacent layers to pack into nearly opposite relative conformations and halide–halide distances between the layers to be shorter. As mentioned previously, shorter halide–halide contacts produce stronger magnetic exchanges. *Bis*(2,3-dimethylpyridinium)tetrabromocuprate(II) is a magnetic ladder with significant exchange interactions. Again, the packing is dictated, in part, by the hydrogen bonding with the pyridinium ion, and by its overall size and shape.

The study of magnetic ladders, such as *bis*(piperidinium)tetrabromocuprate(II) [14] and dibromo-2,3-dimethylpyrazinecopper [15], has been of much interest in recent years because of the observation linking mechanisms in these systems to those that govern high temperature superconductivity [16, 17]. Given the prior success in generating a magnetic ladder using 2,3-dimethylpyridine and the established use of amino substituents to affect packing, there is interest in creating a family of complexes containing 2,3-disubstituted pyridines, including those with the amino group in the 3-position. The effect of changing the position of the hydrogen bonding amino group on the crystal packing and magnetic susceptibility will be explored. We report here the synthesis, structure and magnetic characterization of *bis*(3-amino-2-chloropyridinium)tetrachlorocuprate(II) (**1**) and *bis*(3-amino-2-chloropyridinium)tetrabromocuprate(II) (**2**).

2. Experimental

2.1. *General*

3-Amino-2-chloropyridine, hydrochloric acid and hydrobromic acid were purchased from Aldrich Chemical Company and used without purification. Copper chloride and

copper bromide were obtained from Baker and used without purification. IR spectra were recorded on a Perkin-Elmer FTIR: Paragon 500.

2.2. Bis*(3-amino-2-chloropyridinium)tetrachlorocuprate(II) (1)*

3-Amino-2-chloropyridine (0.645 g, 5.02 mmol) was dissolved in 2 mL of 6 M HCl (12 mmol). Solid $CuCl_2 \cdot 2H_2O$ (0.426 g, 2.50 mmol) was added to the solution followed by an additional 1 mL of 6 M HCl (6 mmol) to ensure complete dissolution. An orange precipitate formed immediately. The mixture was warmed to dissolve the precipitate and the solution was then allowed to cool. Slow evaporation of the dark green aqueous solution at room temperature over the course of eight days gave red crystals of **1** (0.455 g, 39.2%). No attempt was made to maximize the yield. IR (KBr): ν 3401 w, 3321 m, 2853 w, 1624 s, 1543 s, 1465 s, 1368 m, 1315 m, 1134 m, 951 w, 855 w, 792 m, 779 m, 701 cm^{-1}.

2.3. Bis*(3-amino-2-chloropyridinium)tetrabromocuprate(II) (2)*

3-Amino-2-chloropyridine (0.514 g, 4.02 mmol) was dissolved in 3 mL of 4.5N HBr (13.5 mmol). Solid $CuBr_2$ (0.447 g, 2.01 mmol) was added to the solution followed by an additional 2 mL of 4.5 N HBr (9 mmol) to ensure complete dissolution. Slow evaporation of the purple aqueous solution at room temperature over the course of twelve days gave dark purple crystals of **2** (0.320 g, 25.0%). IR (KBr): ν 3401 m, 3305 m, 2928 m, 2864 m, 1624 s, 1542 s, 1465 m, 1366, 1315 m, 1136 m, 1036 w, 941 w, 853 w, 775 m, 699 cm^{-1}.

2.4. *X-ray structure determination*

Data collections were carried out on a Siemens P4 diffractometer employing Mo-Kα radiation ($\lambda = 0.71073$) and a graphite monochromator. Data collection, cell refinement and data reduction were performed using SHELXTL [18]. Absorption corrections were made via redundant data using SADABS [19]. The structures were solved by direct methods and expanded via Fourier techniques [20]. The non-hydrogen atoms were refined anisotropically. Hydrogens bonded to nitrogens were located in the difference maps and their positions were refined using isotropic U values. The aromatic hydrogens were refined via a riding model with fixed isotropic U values. Full crystal and refinement details are given in table 1, while selected bond lengths and angles are given in table 2. Hydrogen bonding parameters are given in table 3. Crystallographic data were used for comparison to powder X-ray diffraction data to establish the purity of the samples used for magnetic studies. The structures have been deposited with the Cambridge Crystallographic Data Centre (**1**, #691642; **2**, #691643).

2.5. *Magnetic susceptibility*

Magnetic data were collected using a Quantum Design MPMS-XL SQUID magnetometer. The 0.0774 g powdered sample of **1** and 0.1104 g powdered sample of **2** used in the magnetic studies were prepared from crushed single crystals. Samples were placed in gelatin capsules and the magnetic moments were measured using magnetic fields of 0 to

Table 1. Crystal data and structure refinement for **1** and **2**.

	1	**2**
Empirical formula	$C_{10}H_{12}N_4Cl_6Cu$	$C_{10}H_{12}N_4Cl_2Br_4Cu$
Formula weight	464.48	642.32
Temperature (K)	262(2)	103(2)
Wavelength (λ, Å)	0.71073	0.71073
Crystal system	Triclinic	Triclinic
Space group	$P\bar{1}$	$P\bar{1}$
Unit cell dimensions (Å, °)		
a	8.8044(4)	9.1110(5)
b	9.3047(4)	9.7069(7)
c	12.5216(5)	12.5707(6)
α	98.940(2)	98.822(4)
β	101.022(2)	100.259(3)
γ	116.664(2)	117.933(2)
V (Å^3)	865.11(6)	929.98(10)
Z	2	2
D_{Calcd} (Mg m^{-3})	1.783	2.294
Absorption coefficient (mm^{-1})	2.184	10.051
$F(000)$	462	606
Crystal size (mm^3)	0.40 × 0.30 × 0.04	0.60 × 0.45 × 0.18
θ Range for data collection (°)	1.72 to 31.59°	1.71 to 31.61°
Limiting indices	$-12 \le h \le 12$, $-13 \le k \le 13$, $-18 \le l \le 18$	$-13 \le h \le 12$, $-13 \le k \le 14$, $-17 \le l \le 17$
Reflections collected	12,457	14,683
Independent reflections	5129 ($R_{int} = 0.0285$)	5570 ($R_{int} = 0.0411$)
Completeness to $\theta = 31.61°$	88.3%	88.9%
Absorption correction	Empirical	None
Max/min transmission	0.9177 and 0.4753	0.2649 and 0.0650
Refinement method	Full-matrix least-squares on F^2	
Data/restraints/parameters	5129/0/208	5570/0/208
Goodness-of-fit on F^2	1.054	1.077
Final R indices [$I > 2\sigma(I)$]	$R_1 = 0.0318$, $wR_2 = 0.0840$	$R_1 = 0.0332$, $wR_2 = 0.0755$
R indices (all data)	$R_1 = 0.0394$, $wR_2 = 0.0918$	$R_1 = 0.0401$, $wR_2 = 0.0782$
Largest difference peak and hole (e Å^{-3})	1.091 and −0.775	2.532 and −1.820

50 kOe at 1.8 K. Several data points were collected as the magnetic field was brought back to 0 kOe to confirm that there was no hysteresis. Temperature dependent magnetic susceptibility data were collected over a temperature range of 1.85–325 K at an applied magnetic field of 1 kOe. The temperature independent diamagnetic correction of the organic base, 3-amino-2-chloropyridine was measured to be -30.2×10^{-6} emu. Diamagentic corrections for the copper and halide ions were taken from Pascal's constants [21]. These corrections and the temperature independent paramagnetic (TIP) correction for copper, 60×10^{-6} cm^3 mol^{-1}, were applied to the data sets.

3. Results and discussion

3.1. *Synthesis*

The reaction of solid $CuCl_2 \cdot 2H_2O$ with two equivalents of 3-amino-2-chloropyridine and excess aqueous HCl gave *bis*(3-amino-2-chloropyridinium)tetrachlorocuprate(II) (**1**)

Table 2. Bond lengths (Å) and angles (°) for **1** and **2**.

1		**2**	
Cu1–Cl1	2.2384(5)	Cu1–Br4	2.3716(5)
Cu1–Cl4	2.2428(5)	Cu1–Br2	2.3739(5)
Cu1–Cl3	2.2651(5)	Cu1–Br3	2.3957(5)
Cu1–Cl2	2.2706(5)	Cu1–Br1	2.4079(5)
N1–C6	1.342(3)	N1–C2	1.338(4)
N1–C2	1.343(2)	N1–C6	1.339(5)
C2–C3	1.397(3)	C2–C3	1.394(5)
C2–Cl5	1.7069(19)	C2–Cl1	1.710(3)
C3–N3	1.344(3)	C3–N3	1.347(5)
C3–C4	1.411(3)	C3–C4	1.407(5)
Cl1–Cu1–Cl4	96.627(19)	Br4–Cu1–Br2	96.085(18)
Cl1–Cu1–Cl3	97.354(19)	Br4–Cu1–Br3	96.773(19)
Cl4–Cu1–Cl3	140.63(2)	Br2–Cu1–Br3	140.26(2)
Cl1–Cu1–Cl2	139.38(2)	Br4–Cu1–Br1	138.94(2)
Cl4–Cu1–Cl2	96.277(18)	Br2–Cu1–Br1	97.368(18)
Cl3–Cu1–Cl2	96.592(19)	Br3–Cu1–Br1	97.153(17)
C6–N1–C2	123.12(19)	C2–N1–C6	123.3(3)
N1–C2–C3	120.76(18)	N1–C2–C3	120.7(3)
N1–C2–Cl5	117.66(15)	N1–C2–Cl1	117.4(3)
C3–C2–Cl5	121.58(14)	C3–C2–Cl1	121.8(3)
N3–C3–C2	121.39(19)	N3–C3–C2	121.1(3)
N3–C3–C4	122.2(2)	N3–C3–C4	122.5(3)
C2–C3–C4	116.43(18)	C2–C3–C4	116.4(3)
C5–C4–C3	120.9(2)	C5–C4–C3	120.8(3)
C4–C5–C6	120.00(19)	C4–C5–C6	120.3(3)
N1–C6–C5	118.79(19)	N1–C6–C5	118.4(3)

Table 3. Hydrogen bonds for **1** and **2** (Å and °).

For **1**				
D–H···A	d(D–H)	d(H···A)	d(D···A)	∠(DHA)
N1–H1···Cl2#1	0.84(3)	2.29(3)	3.1047(18)	161(3)
N3–H3A···Cl1#2	0.85(4)	2.46(4)	3.305(2)	171(3)
N3–H3B···Cl1	0.84(4)	2.52(4)	3.324(2)	160(3)
N11–H11···Cl3#3	0.78(3)	2.36(3)	3.1053(18)	162(3)
N13–H13A···Cl4#4	0.85(3)	2.53(3)	3.353(2)	162(3)
For **2**				
D–H···A	d(D–H)	d(H···A)	d(D···A)	∠(DHA)
N1–H1···Br1	0.79(5)	2.50(5)	3.244(3)	158(4)
N3–H3A···Br4#1	0.85(6)	2.64(7)	3.424(4)	154(5)
N3–H3B···Br4#2	0.76(6)	2.71(7)	3.432(4)	160(6)
N11–H11···Br3#3	0.84(5)	2.51(5)	3.260(3)	151(4)
N13–H13B···Br2#4	0.82(5)	2.68(5)	3.485(4)	170(5)

Symmetry transformations used to generate equivalent atoms: **1**: #1 $x, y+1, z$; #2 $-x, -y+1, -z$; #3 $-x+1, -y+1, -z+1$; #4 $x-1, y, z$; **2**: #1 $x, y-1, z$; #2 $-x-1, -y-1, -z$; #3 $-x, -y, -z+1$; #4 $x-1, y, z$.

in 39.2% yield. Red crystals suitable for X-ray diffraction crystallized upon slow evaporation at room temperature over the course of eight days. Similarly, *bis*(3-amino-2-chloropyridinium)tetrabromocuprate(II) (**2**), prepared from solid $CuBr_2$, two equivalents of 3-amino-2-chloropyridine, and excess aqueous HBr, crystallized over the course

of twelve days as deep purple crystals in 25% yield.

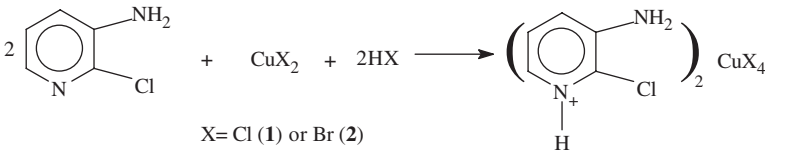

3.2. *Analysis of crystal structures*

Compounds **1** and **2** both occur as triclinic crystals in the space group $P\bar{1}$. Crystallographic data for both compounds are given in table 1. Selected bond lengths and angles are given in table 2. Table 3 lists the hydrogen bonding parameters. Both compounds contain distorted CuX_4^{2-} ions. A common measure of the degree of distortion is to calculate the mean *trans* angle, or the average of the two large X–Cu–X angles; idealized tetrahedral and square planar molecules have bond angles of 109.5° and 180°, respectively.

3.2.1. X-ray structure of *bis*(3-amino-2-chloropyridinium)tetrachlorocuprate(II) (1). The asymmetric unit of **1** is shown in figure 1. The $CuCl_4^{2-}$ ions are highly distorted with a mean *trans* angle of 140°; there is a nearly uniform distortion about the copper with the large Cl–Cu–Cl angles being 139.4° and 140.6°. The bond lengths and angles for the 3-amino-2-chloropyridinium ions are comparable to those of the related 3-amino-2-chloropyridinium complex – 3-amino-2-chloropyridinium dihydrogenphosphate [22]. The copper chloride bond lengths are normal, averaging 2.2542(5) Å. The cations are nearly planar with mean deviations of 0.002 Å and 0.00051 Å from the plane for the N1 and N11 rings, respectively. The amino and chloro substituents are almost co-planar

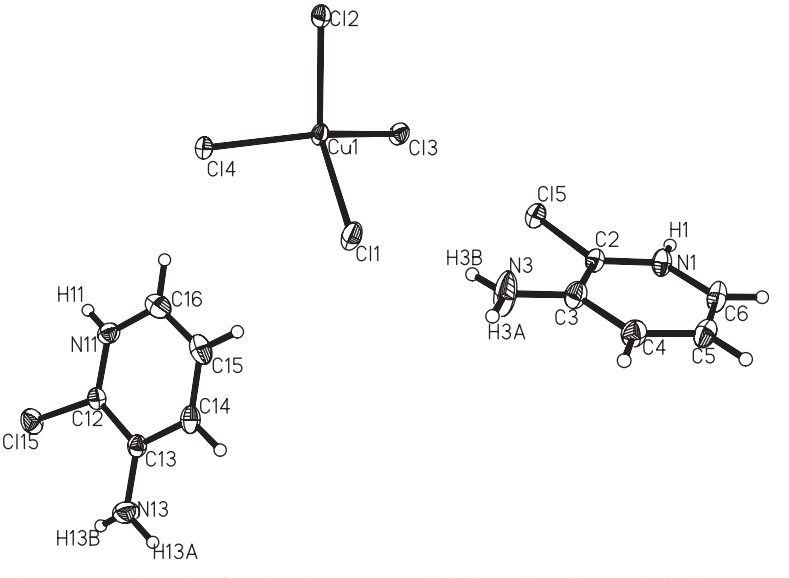

Figure 1. The asymmetric unit of **1** showing 50% probability ellipsoids. Only hydrogen atoms which positions were defined are labeled.

with the rings, but are bent slightly to opposite sides of the plane. The planes of the amino groups (N3, H3A, H3B and N13, H13A, H13B) are rotated 3° and 5.3° relative to the pyridinium rings. The two cations are canted 63.8° to each other.

Molecules of **1** pack in the lattice to generate layers of $CuCl_4^{2-}$ anions parallel to the *ac*-face, which are separated by two layers of 3-amino-2-chloropyridinium cations (figure 2). One layer of cations lies parallel to the *bc*-face diagonal while the other stacks parallel to the *a*-axis.

Each Cl1 forms hydrogen bonds to two amino hydrogens ($d_{N3–H3A\cdots Cl1} = 3.305$ Å, ∠171°; $d_{N3–H3B\cdots Cl1} = 3.324$ Å, ∠160°), the second of which is an intramolecular hydrogen bond. The pyridinium hydrogens form hydrogen bonds to Cl2 and Cl3: $d_{N1–H1\cdots Cl2} = 3.1047$ Å, ∠161°; $d_{N11–H11\cdots Cl3} = 3.1053$ Å, ∠162°. Only one hydrogen in the amino group of the N11 pyridinium ring forms a hydrogen bond: $d_{N13–H13A\cdots Cl4} = 3.353$ Å, ∠162°.

The $CuCl_4^{2-}$ anions form a linear chain parallel to the *a*-axis (figure 3). The separation between successive copper halide ions is 4.595 Å, representing the closest Cl···Cl non-bonding contact. The Cu1–Cl1–Cl2A angle is 156.4° and the Cu1A–Cl2A–Cl1 angle is

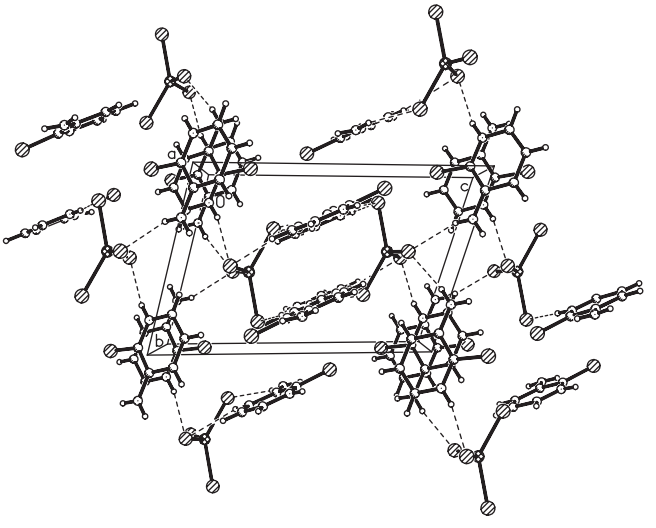

Figure 2. Packing diagram of **1** showing the two orientations of the cations. Dashed lines indicate hydrogen bonds.

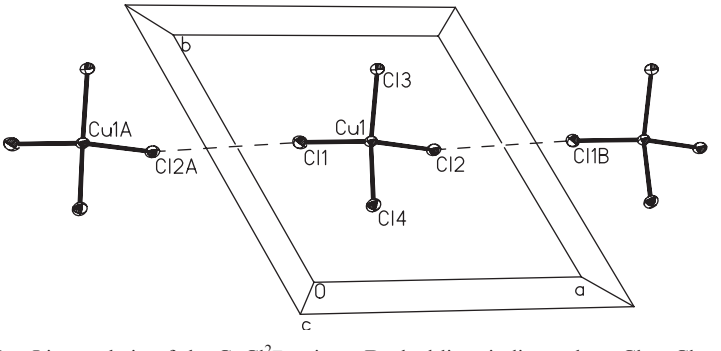

Figure 3. Linear chain of the $CuCl_4^{2-}$ anions. Dashed lines indicate short Cl···Cl contacts.

160.5°. The torsion angle, Cu1–Cl1–Cl2A–Cu1A, between adjacent $CuCl_4^{2-}$ ions is 38.5°. The next closest interaction has a Cl···Cl separation of 4.851 Å.

3.2.2. X-ray structure of bis(3-amino-2-chloropyridinium)tetrabromocuprate(II) (2). Compound **2** also crystallizes in the triclinic space group $P\bar{1}$. The asymmetric unit is shown in figure 4. The $CuBr_4^{2-}$ ions are highly distorted with a mean *trans* angle of 139.6°. The bond lengths and angles for the 3-amino-2-chloropyridinium cations are comparable to those in **1** and thus also to those in 3-amino-2-chloropyridinium dihydrogenphosphate [22]. The copper bromide bond lengths are normal, averaging 2.3873(5) Å, and are slightly longer than the corresponding Cu–Cl bond lengths as expected. The cations are nearly planar with mean deviations of 0.0044 Å and 0.0076 Å from the plane for the N1 and N11 rings, respectively. Similar to **1** the amino and chloro substituents are almost co-planar with the rings, but are canted toward opposite sides of the plane. The amino groups (N3 and N13) are rotated 11.1° and 8.7° relative to the pyridinium rings. The two cations are canted 60.9° to each other.

Molecules of **2** also pack in the lattice to form layers of $CuBr_4^{2-}$ parallel to the *ac*-face, which are separated by two different layers of cations. The packing diagram of **2** is therefore very similar to **1**. There is close contact between the pyridinium chlorine and a bromide from $CuBr_4^{2-}$ (figure 5). This close contact has been found in many metal-organic salts and is believed to influence the crystal packing of the salts [23]. The Cl···Br^- separation distance, 3.677 Å, is less than the sum of the van der Waals radii of the chlorine and the ionic radius of bromide. The C–Cl···Br^- has an angle of 165.1° which is within the range of bond angles listed in Awwadi *et al.* [23]. The Cu–Br···Cl angle is 101.3° and the torsion angle, Cu1–Br3···Cl1–C2, is −1.7°. Examination of the structure of **1** shows a similar interaction with nearly identical parameters except for the halogen–halide distance: Cl···Cl^-, 3.44 Å; Cu–Cl···Cl, 101.3°; C–Cl···Br, 165.2; Cu1–Cl3···Cl5–C2, −1.7°.

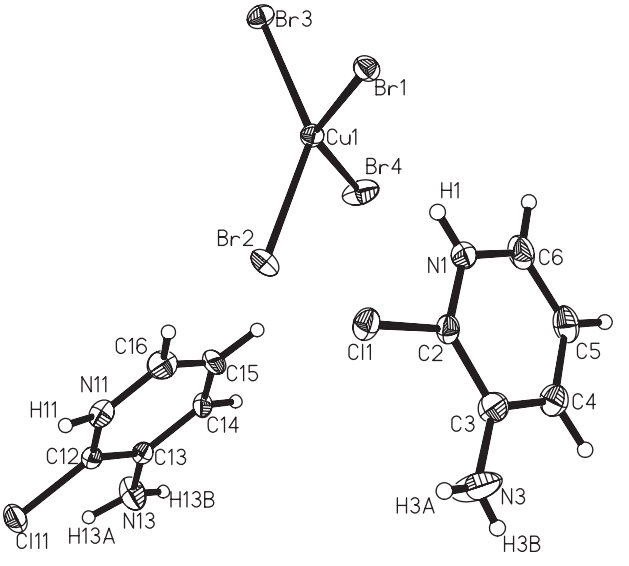

Figure 4. The asymmetric unit of **2** showing 50% probability ellipsoids. Only hydrogen atoms which positions were defined are labeled.

The hydrogen bonding scheme of **2** is similar to **1** (see table 3). The pyridinium hydrogens form hydrogen bonds to Br1 and Br3: $d_{N1\text{-}H1\cdots Br1} = 3.244$ Å, ∠158°; $d_{N11\text{–}H11\cdots Br3} = 3.260$ Å, ∠151°. Each Br4 forms hydrogen bonds to two amino hydrogens: $d_{N3\text{–}H3A\cdots Br4} = 3.424$ Å, ∠154°; $d_{N3\text{-}H3B\cdots Br4} = 3.432$ Å, ∠160°. Only one hydrogen in the amino group of the N11 pyridinium ring forms hydrogen bonds: $d_{N13\text{–}H13B\cdots Br2} = 3.485$ Å, ∠170°. As expected, the hydrogen bond lengths of **2** are longer than those of **1**.

The $CuBr_4^{2-}$ anions form layers parallel to the *b*-face (figure 6). The closest Br1–Br4F non-bonding contact distance is 4.652 Å forming a chain of $CuBr_4^{2-}$ ions. The next closest interaction is from Br1–Br4B with a separation distance of 4.682 Å. Together these contacts form a ladder. However, neighboring ladders are not completely isolated; the Br3-Br2C contact has a separation of 4.912 Å, within the range of separations shown to play a role in magnetic exchange pathways. *Bis*(2-amino-5-methylpyridinium)tetrabromocuprate(II), which forms a square lattice, has contact distances of 4.55 Å and 4.97 Å [24].

3.3. *Magnetic susceptibility*

Magnetic susceptibility data were obtained on powdered samples using a Quantum Design SQUID magnetometer. The molar susceptibility, χ_{mol} ($\chi_{mol} = \lim_{B\to 0} M/B$) was

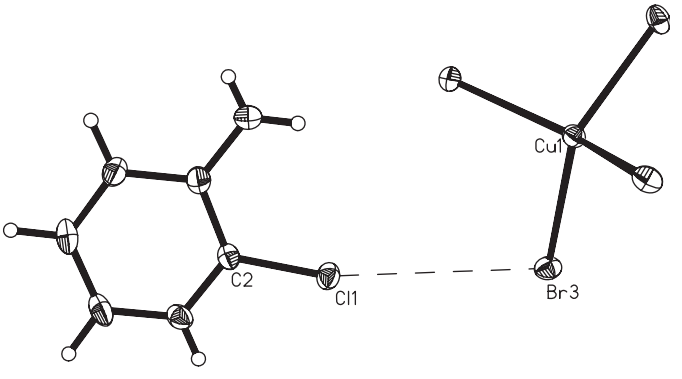

Figure 5. Close contact between the pyridinium chlorine and a bromide from a $CuBr_4^{2-}$ ion.

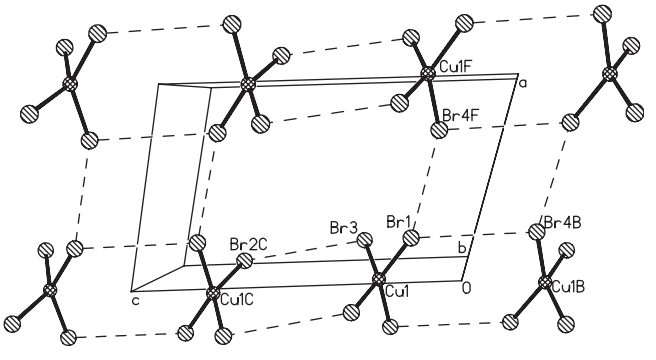

Figure 6. Layers of the $CuBr_4^{2-}$ anions in **2**. Dashed lines represent short Br···Br contacts. The Br1–Br4F separation is 4.652 Å, the Br1–Br4B separation is 4.682 Å, and the Br3–Br2C separation is 4.912 Å.

collected as a function of temperature between 1.85 and 325 K for **1** and **2**. Corrections to molar susceptibility were applied for the temperature-independent magnetization of the Cu(II) (60×10^{-6} emu mol^{-1}) and the diamagnetic contributions (-157.66×10^{-6} and -199.66×10^{-6} emu mol^{-1} for the chloride and bromide salts, respectively). Initial corrections made using Pascal's constants (-247.1×10^{-6} and -289.1×10^{-6} emu mol^{-1} for **1** and **2**, respectively) gave values for χT which showed a monotonic increase at high temperatures. Therefore, the diamagnetic contributions were recalculated using Pascal's constants for the copper and halide ions, and an experimentally measured value for the organic base (-30.2×10^{-6} emu). The diamagnetic correction used for **1** was 63.8% of the initial calculation and that of **2** 69.1% of the initial correction. This change in the diamagnetic correction resulted in the expected behavior of the χT *versus* T plot. All data were interpreted with the following Hamiltonian: $H = -2J \sum \vec{S}_i \cdot \vec{S}_j$.

The χ^{-1} *versus* T data plots for **1** and **2** indicate weak antiferromagnetic interactions, shown by the small negative theta values (**1**: −0.517; **2**: −2.22) extrapolated from the high temperature portions of the plots. The χT *versus* T plot (figure 7) shows that the Curie constant for **1** is about 0.45 emu*K mol^{-1} while the plot for **2** (figure 8) gives a Curie constant of 0.41 emu*K mol^{-1}.

The χ *versus* T plot for **1** (figure 7) was fit to a uniform linear antiferromagnetic chain model [25]. Attempts to fit the data to other models including a dimer and two different ladder models gave poor results or unrealistic parameters such as negative percent impurities. The linear chain model gave 0.448(3) for the Curie constant and −1.3(5) for $2J\,k^{-1}$ with an R^2 of 0.99996. Due to the weakness of the interactions, the system approximates a simple paramagnet and similar values were obtained with percent paramagnetic impurity values ranging from zero to 50%, even though powder X-ray diffraction did not show any impurities in the sample.

The χ *versus* T plot for **2** (figure 9) was fit to a two-dimensional antiferromagnetic layer model [26, 27]. Attempts to fit it to a linear chain and two different ladder models gave poor results or unrealistic parameters. Table 4 summarizes the

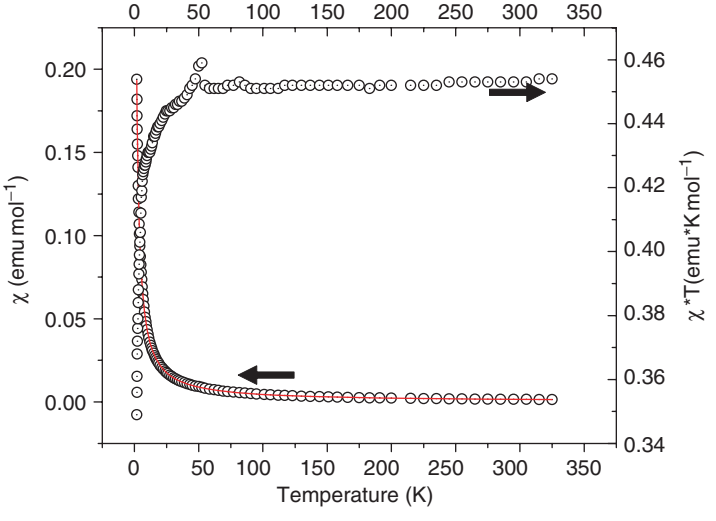

Figure 7. χ *vs.* T and χT *vs.* T plots for **1**. χ *vs.* T plot is fitted to a Heisenberg S = ½ linear chain model. The anomaly at 50 K in the χT *vs.* T plot is due to trace molecular O_2 in the sample.

Curie constant, exchange constant, paramagnetic impurity and R^2 values of the all the models used. Although the two shortest contact distances form a ladder of $CuBr_4^{2-}$ ions, the close contact between neighboring ladders clearly has a significant role in the exchange pathway based upon the results of the magnetic data. While the R^2 value for the strong rail ladder model (0.99996) may statistically represent a good

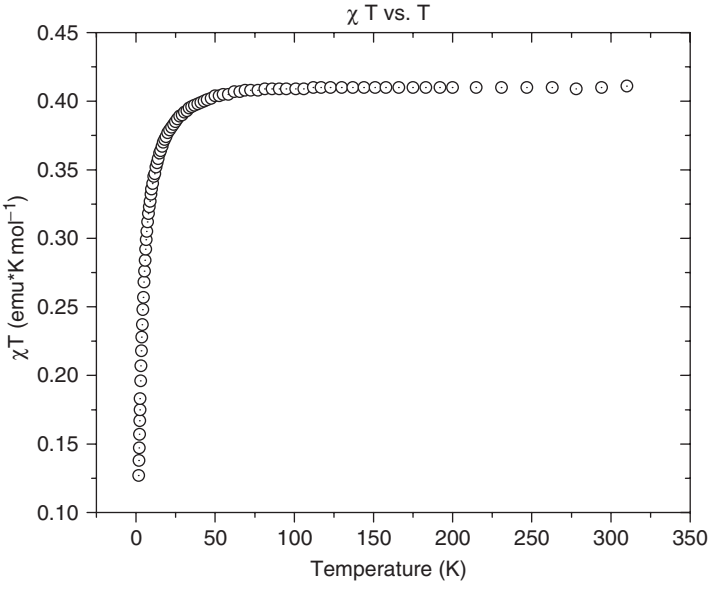

Figure 8. χT *vs.* T plot for **2**.

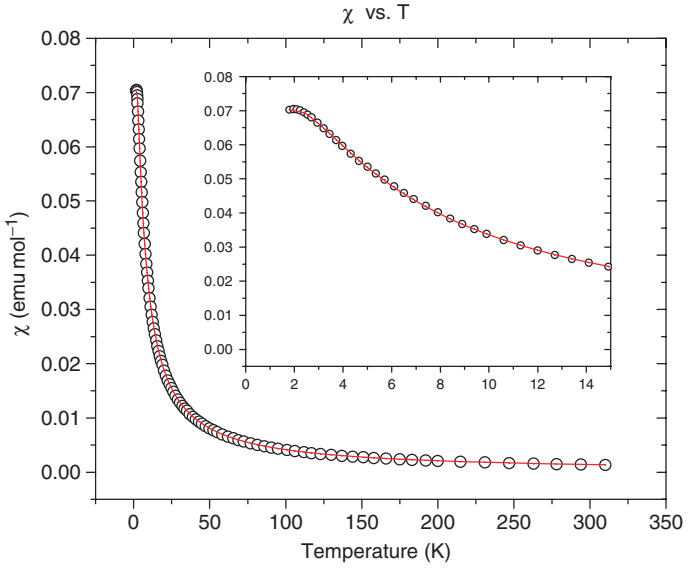

Figure 9. χ *vs.* T plot for **2**. The line shows the fit to an S = ½ 2-D Heisenberg antiferromagnetic layer. The inset is the expansion of the fit at low temperatures.

Table 4. Data from models used to fit **2**.

Model	Curie C	$2J\,k^{-1}$ (K)	$2J'\,k^{-1}$ (K)	Impurity (%)	R^2
Layer	0.425	−2.48	–	4.5	0.99998
Ladder (strong rung)	0.414	−2.94 (rail)	−2.25 (rung)	1.9×10^{-3}	0.9972
Ladder	0.416	−4.00 (rail)	−2.62 (rung)	−6.5 0	0.99997
(strong rail)	0.415	−4.12 (rail)	−2.08 (rung)		0.99996
Linear Chain	0.411	−3.95	–	7.1	0.99992

Table 5. Short contact distances and angles of $CuBr_4^{2-}$ anions (**2**) (see figure 6 for labeling).

Contacts	d(Br···Br)Å	θ_1 (°) Cu– Br···Br	θ_2 (°) Br···Br–Cu	τ (°) Cu–Br···Br–Cu
Cu1–Br1···Br4F–Cu1F	$d_1 = 4.652$	160.1	156.7	35.4
Cu1–Br1···Br4B–Cu1B	$d_2 = 4.682$	126.1	94.9	−2.4
Cu1–Br3···Br2C–Cu1C	$d_3 = 4.912$	84.9	134.6	4.8

fit, it deviates from the curve at low temperature. The 2-D layer model resulted in the best fit of the curve, especially in the low temperature portion of the curve (see inset of figure 9). Referring to table 5, which lists the short contact distances, angles and torsion angles between the $CuBr_4^{2-}$ anions, the first two contacts are comparable, but the third is about 9.5% longer than the other two. However, as mentioned previously, this contact distance is still within the normal range of separation in which exchange pathways are seen. Therefore, the magnetic data show that the structure dictates a 2-D layer.

4. Conclusions

The *bis*(3-amino-2-chloropyridinium)tetrachlorocuprate and tetrabromocuprate salts crystallize in the triclinic space group Pī. Both compounds exhibit weak antiferromagnetic interactions. The magnetic data for **1** best fits a linear chain model. The magnetic data for **2** best fits the model of a two-dimensional antiferromagnetic layer. Work using other 2,3-disubstituted pyridine bases is in progress.

Acknowledgements

S.N.H. received financial support through a Maurine H. Milburn Summer Research Fellowship and a Fredrick and Alice Murdock Summer Research Fellowship. Funding for the powder X-ray diffractometer and SQUID magnetometer was provided by a Kresge Foundation grant, PolyCarbon Industries Inc., and the National Science Foundation. The authors are indebted to Dr. Robert T. Butcher for his assistance with processing SQUID data.

References

[1] (a) K. Halvorson, R.D. Willett. *Acta Crystallogr., Sect. C*, **44**, 2071 (1988); (b) G.V. Rubenacker, J.E. Drumheller. *J. Magn. Magn. Mater.*, **79**, 119 (1989); (c) P. Zhou, J.E. Drumheller. *J. Appl. Phys.*, **67**, 5755 (1990).
[2] H. Place, R.D. Willett. *Acta Crystallogr., Sect. C*, **43**, 1050 (1987).
[3] (a) T. Manfredini, G.C. Pellacani, A. Bonamartini-Corradi, L.P. Battaglia, G.G.T. Gaurini, J.G. Guisti, R.D. Willett, D.X. West. *Inorg. Chem.*, **29**, 221 (1990); (b) C. Zanchini, R.D. Willett. *Inorg. Chem.*, **29**, 3027 (1990).
[4] R.L. Carlin. *Magnetochemistry*, Springer-Verlag, Berlin, Heidelberg, Germany (1986).
[5] G. Marcotrigiano, L. Menabue, G.C. Pellacani. *J. Coord. Chem.*, **9**, 141 (1979).
[6] C.-K. Jeong, Y.-I. Kim, S.-N. Choi. *Bull. Korean Chem. Soc.*, **17**, 845 (1996).
[7] L.A. Doadrio, M.T. Gutierez Rios. *An. Quim.*, **75**, 228 (1979).
[8] L.O. Snively, G.F. Tuthill, J.E. Drumheller. *Phys. Rev. B*, **24**, 5349 (1981).
[9] F.M. Woodward, C.P. Landee, J. Giantsidis, M.M. Turnbull, C. Richardson. *Inorg. Chim. Acta*, **324**, 324 (2001).
[10] F.M. Woodward, A.S. Albrecht, C.M. Wynn, C.P. Landee, M.M. Turnbull. *Phys. Rev. B*, **65**, 144412 (2002).
[11] T.J. Coffey, C.P. Landee, W.T. Robinson, M.M. Turnbull, M. Winn, F.M. Woodward. *Inorg. Chim. Acta*, **303**, 54 (2000).
[12] R. Willett, H. Place, M. Middleton. *J. Am. Chem. Soc.*, **26**, 8639 (1988).
[13] A. Shapiro, C.P. Landee, M.M. Turnbull, J. Jornet, M. Deumal, J.J. Novoa, M.A. Robb, W. Lewis. *J. Am. Chem. Soc.*, **129**, 952 (2007).
[14] B.C. Watson, V.N. Kotov, M.W. Meisel, D.W. Hall, G.E. Granroth, W.T. Montfrooij, S.E. Nagler, D.A. Jensen, R. Backov, M.A. Petruska, G.E. Fanucci, D.R. Talham. *Phys. Rev. Lett.*, **86**, 5168 (2001).
[15] B.M. Wells, C.P. Landee, M.M. Turnbull, F.F. Awwadi, B. Twamley. *J. Mol. Catal. A: Chem.*, **228**, 117 (2005).
[16] E. Dagotto. *Rep. Prog. Phys.*, **62**, 1525 (1999).
[17] S. Sachdev. *Science*, **288**, 475 (2000).
[18] G.M. Sheldrick. *SHELXTL: v. 5.10, Structure Determination Software Suite*, Bruker AXS Inc., Madison, WI (2001).
[19] G.M. Sheldrick. *SADABS. Program for Empirical Absorption Correction of Area Detector Data*, University of Göttingen, Germany (1996).
[20] G.M. Sheldrick. *SHELX97-2. Programs for the Solution and Refinement of Crystal Structures*, University of Göttingen, Germany (1997).
[21] R.L. Carlin. *Magnetochemistry*, Springer-Verlag, Berlin, Heidelberg, Germany (1986).
[22] K. Hamed, A. Samah, R. Mohamed. *Acta Crystallogr., Sect. E: Struct. Rep. Online*, **63**, 2896 (2007).
[23] F.F. Awwadi, R.D. Willett, B. Twamley. *Cryst. Growth Des.*, **7**, 624 (2007).
[24] M.M. Turnbull, C.P. Landee, B.M. Wells. *Coord. Chem. Revi.*, **249**, 2567 (2005).
[25] D.C. Johnston, R.K. Kremer, M. Troyer, X. Wang, A. Klumper, S.L. Bud'ko, A.F. Panchula, P.C. Canfield. *Phys. Rev. B*, **61**, 9558 (2000).
[26] L.J. de Jongh. In *Magnetic Properties of Layered Transition Metal Compounds*, L.J. de Jongh (Ed.), Kluwer Academic, Hingham, MA (1989).
[27] J. Kim, M. Troyer. *Phys. Rev. Lett.*, **80**, 2705 (1998).